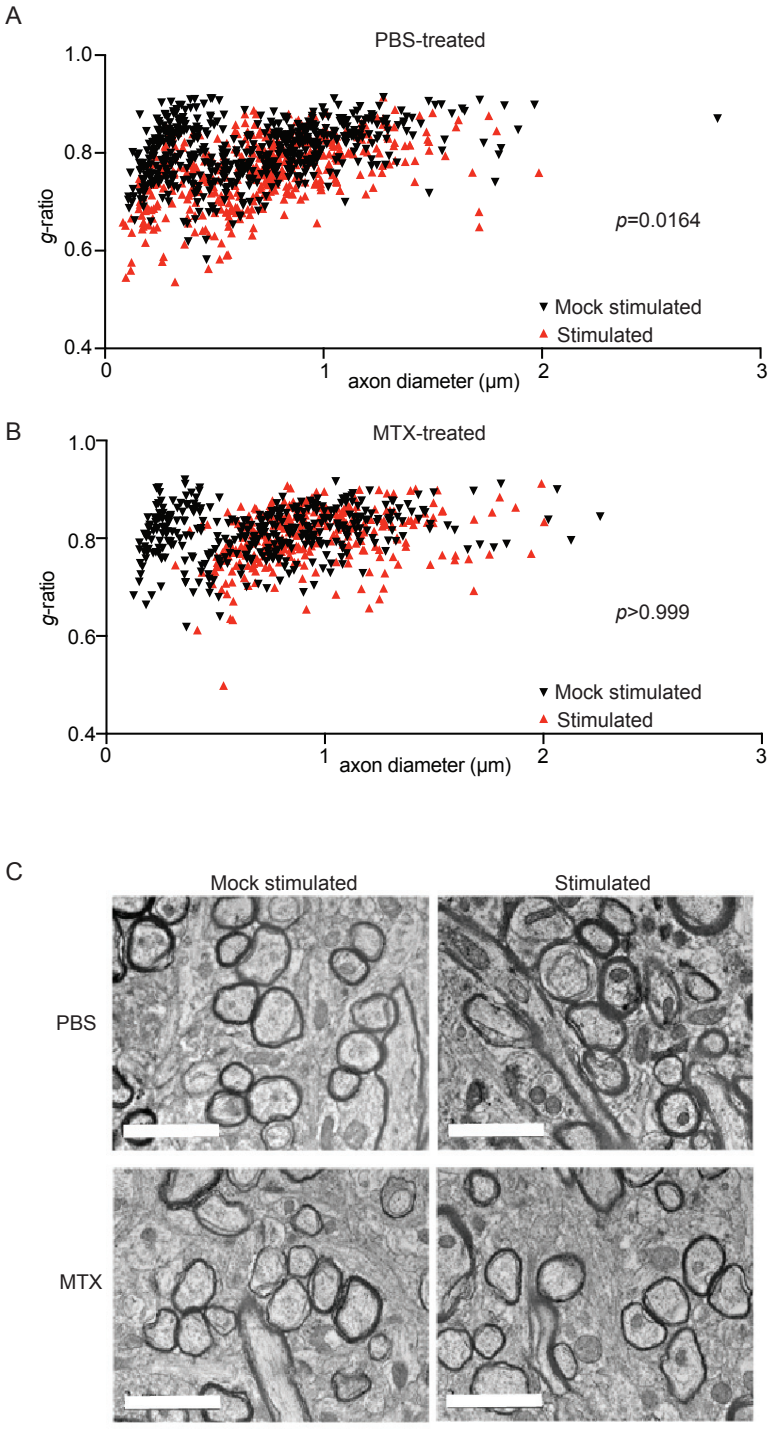

Supplemental Fig 1. Failure of adaptive myelination in a mouse model of MTX chemotherapy-related cognitive dysfunction, related to Figure 1

These data represent an independent replicate of the data presented in Figure 1. In this experiment, the tissue processed for transmission electron microscopy (TEM) exhibited more split artifact than typically observed. Given the technical issue, we replicated the experiment entirely (presented in

Figure 1). The data presented here in Fig. S1 demonstrated the same failure of activity-regulated myelination following methotrexate as observed in the more technically sound analyses in Fig. 1.

A-B) TEM was performed one month following the cessation of the 7-day optogenetic stimulation paradigm in *Thy1::ChR2*$^{+/-}$ mice that were either stimulated or identically manipulated with the exception of blue light exposure (mock-stimulated controls). These *Thy1::ChR2*$^{+/-}$ mice were previously exposed to MTX or PBS vehicle control, resulting in four experimental groups. The *g*-ratio data are shown as a function of axon caliber as a scatterplot of all axons measured in (A) PBS vehicle control-treated, mock-stimulated mice (n= 6 mice; black triangles) compared to PBS vehicle control-treated, optogenetically stimulated mice (n= 5 mice; red triangles) and in (B) MTX-treated, unstimulated mice (n= 4 mice; black triangles) compared to MTX-treated, optogenetically stimulated mice (n= 3 mice; red triangles). A single point indicates the *g*-ratio for a single axon. Approximately 100 axons were quantified and the mean g-ratio determined for each mouse. P-values (indicated on plots) were determined by a two-way ANOVA with Bonferoni correction for multiple comparisons, comparing the mean *g*-ratio per mouse between groups.

C) Representative TEM images of premotor projections entering the subjacent corpus callosum at the level of the cingulum. Scale bars=2μm.

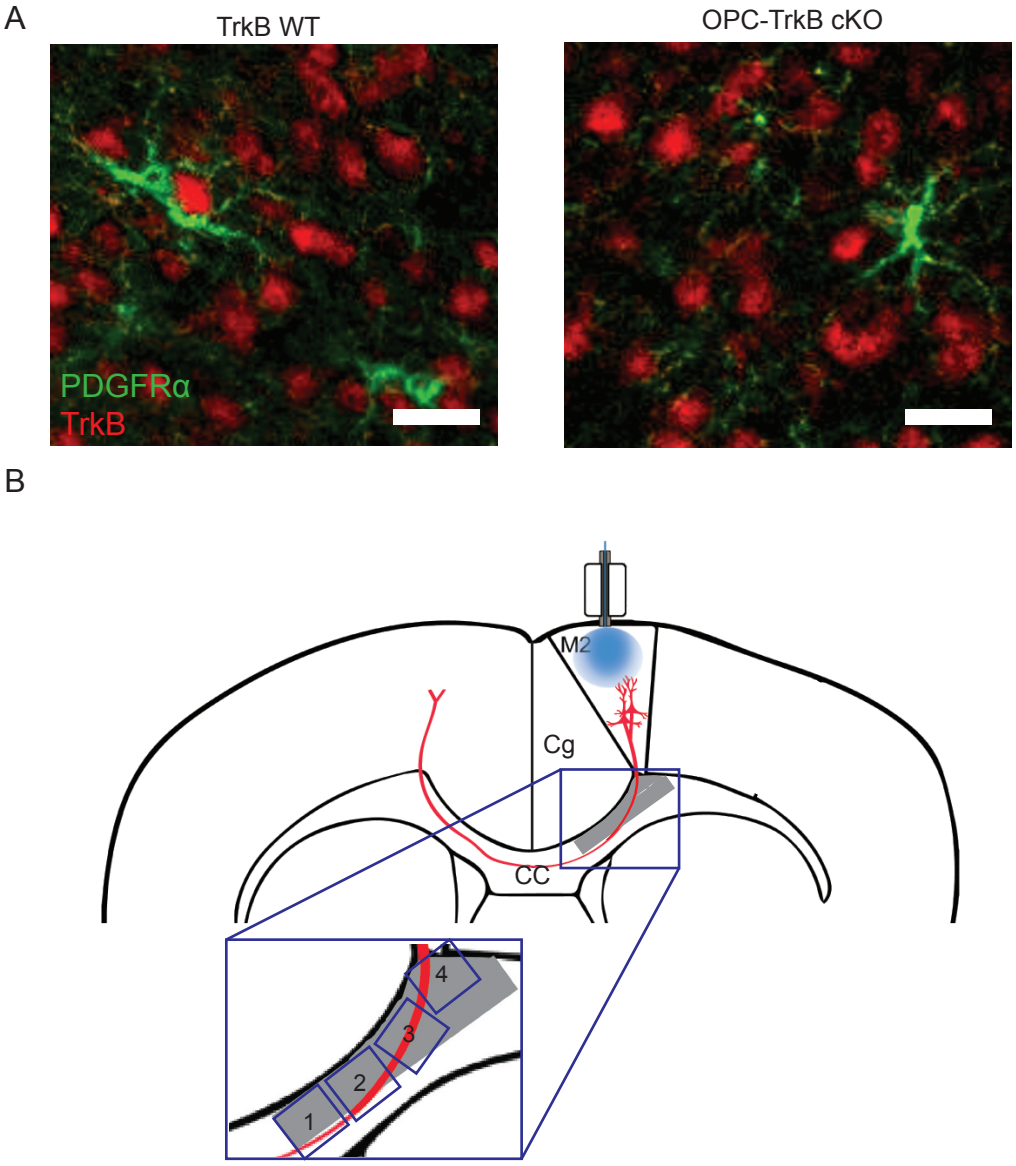

Supplemental Fig 2. Verification of conditional TrkB knockout in OPCs and standardized region of cell density quantification, related to Figure 3, S3

A) Representative confocal images of TrkB (red) expression in PDGFRα+ OPCs (green), assessed by immunohistochemistry. TrkB is expressed in TrkB WT OPCs (left), and following tamoxifen induction TrkB expression is lost from OPCs in TrkB cKO mice (right). Scale bar = 10μm

B) Standardized fields (blue squares) sampled in the corpus callosum for all cell density measurements.

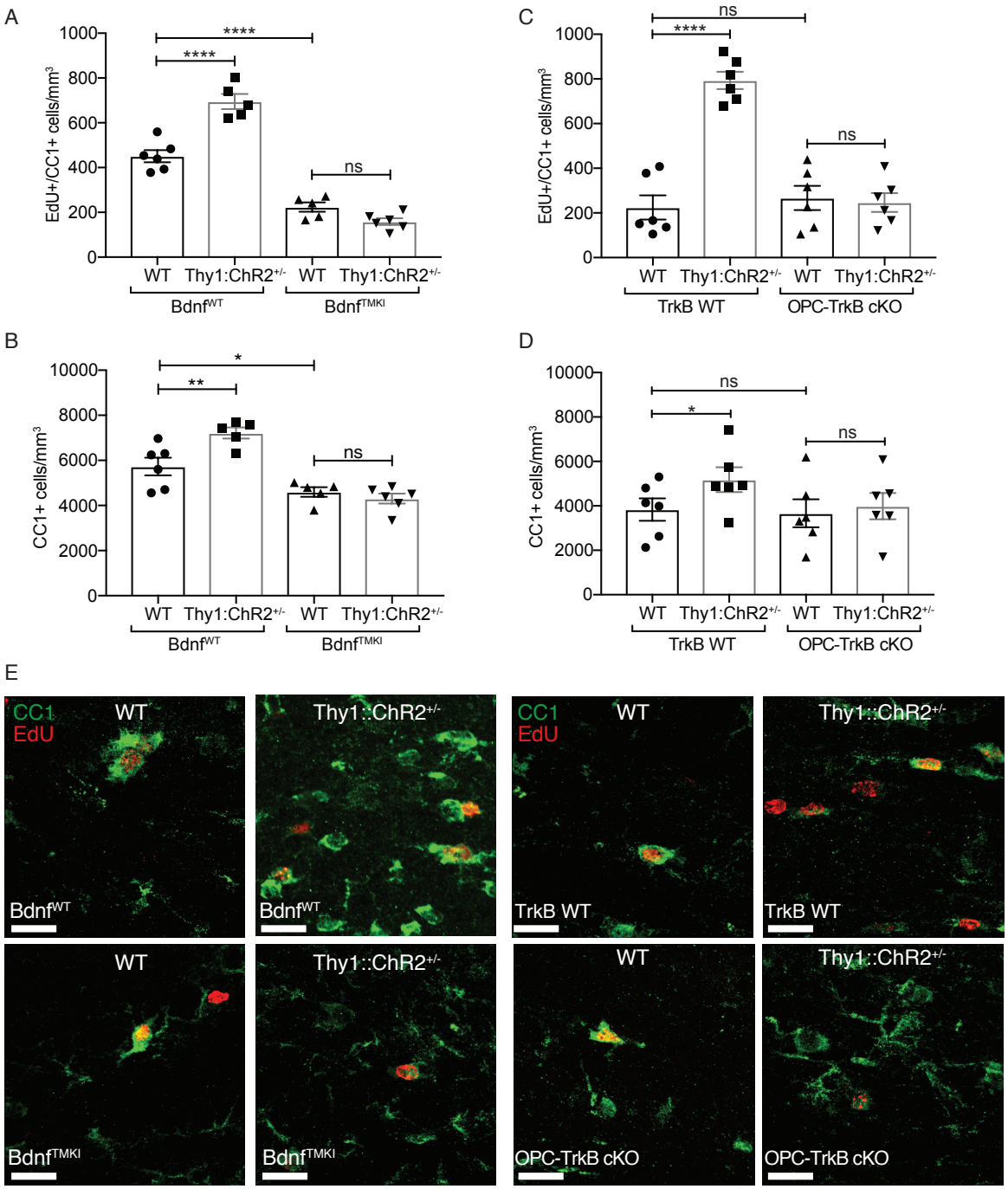

Supplemental Fig 3. BDNF to TrkB signaling is necessary for activity-regulated oligodendrogenesis, related to Figures 3, 4 and S2

A) Density of EdU-marked oligodendrocytes ($EdU^+/CC1^+$ cells) in corpus callosum of *$Bdnf^{TMKI}$;Thy1::$ChR2^{+/-}$* mice (n=5), *$Bdnf^{TMKI}$;*WT mice (n=6), *$Bdnf^{WT}$;Thy1::$ChR2^{+/-}$* mice (n = 6) and *$Bdnf^{WT}$;*WT mice (n=5) at 4 weeks after completion of the 7-day optogenetic stimulation paradigm.

B) Density of total $CC1^+$ oligodendrocytes in the corpus callosum of *$Bdnf^{TMKI}$;Thy1::$ChR2^{+/-}$* mice (n=5), *$Bdnf^{TMKI}$;*WT mice (n=6), *$Bdnf^{WT}$;Thy1::$ChR2^{+/-}$* mice (n = 6) and *$Bdnf^{WT}$;*WT mice (n=5) at 4 weeks after completion of the 7-day optogenetic stimulation paradigm.

C) Density of EdU-marked oligodendrocytes ($EdU^+/CC1^+$ cells) in the corpus callosum of OPC TrkB cKO*;Thy1::$ChR2^{+/-}$* mice (n=6), OPC TrkB cKO;WT (no opsin) mice (n=6), TrkB WT*;Thy1::$ChR2^{+/-}$* mice (n=6) and TrkB WT;WT (no opsin) mice (n=6) at 4 weeks after completion of the 7-day optogenetic stimulation paradigm.

D) Density of total $CC1^+$ oligodendrocytes in the corpus callosum of OPC TrkB cKO*;Thy1::$ChR2^{+/-}$* mice (n=6), OPC TrkB cKO;WT (no opsin) mice (n=6), TrkB WT*;Thy1::$ChR2^{+/-}$* mice (n=6) and TrkB WT;WT (no opsin) mice (n=6) at 4 weeks after completion of the 7-day optogenetic stimulation paradigm.

E) Representative confocal images of oligodendrocytes ($CC1^+$, green) co-localized with EdU (red) in the corpus callosum for each group described above. Scale bar = 20μm.

Data shown as mean ± SEM. Each point = one mouse. ns = $p > 0.05$, *$p<0.05$, **$p < 0.01$ ****$p<0.0001$. Two-way ANOVA with Tukey post-hoc analysis for multiple comparisons.

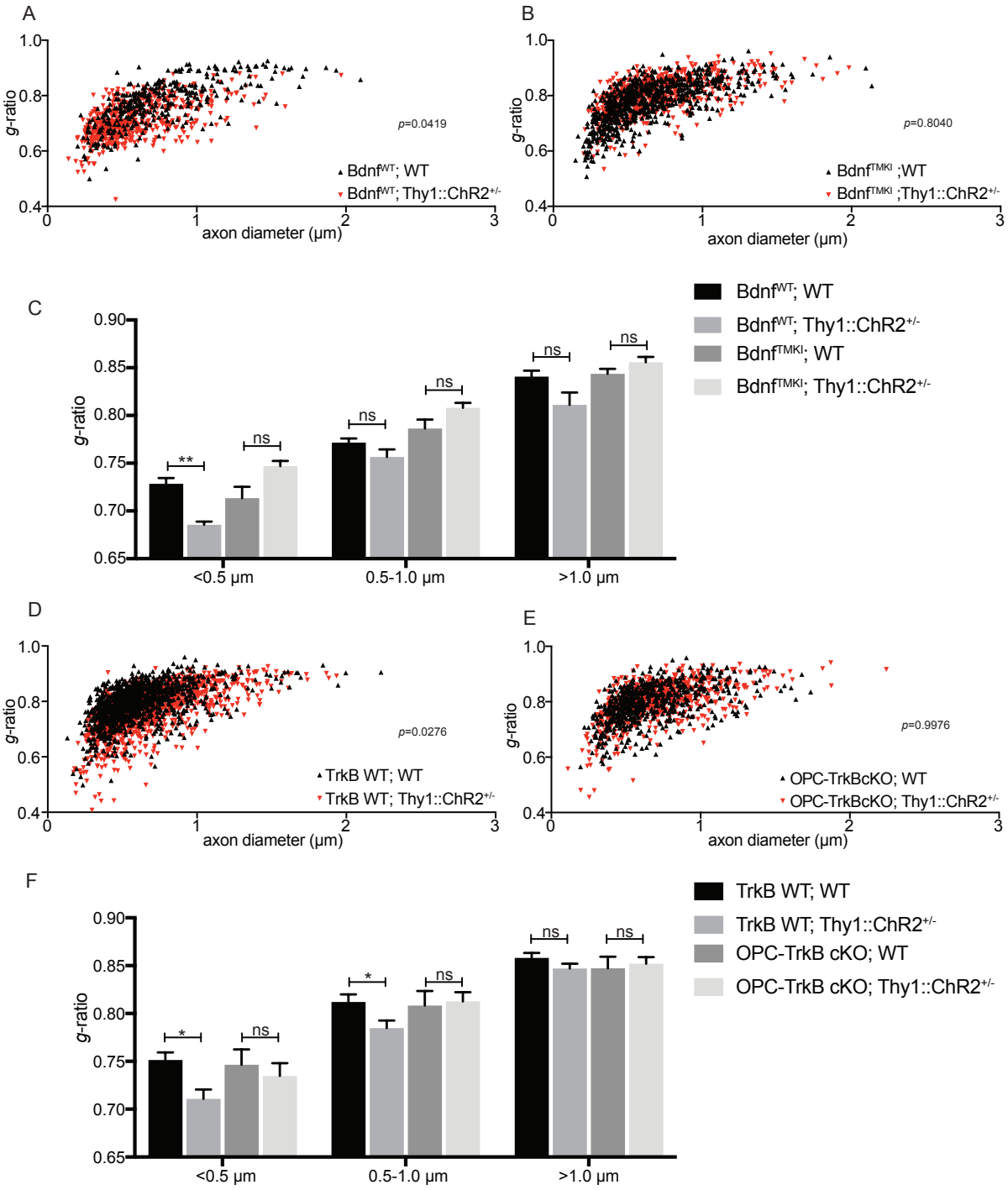

Supplemental Fig 4. BDNF to TrkB signaling is necessary for activity-regulated myelination, related to Figure 4

Transmission electron microscopy (TEM) was performed 4-weeks following the cessation of the 7-day optogenetic stimulation paradigm. Myelin sheath thickness was analyzed at the level of the cingulum of the corpus callosum as the *g*-ratio (diameter of axon divided by the diameter of axon plus myelin sheath; a smaller *g*-ratio indicates a thicker myelin sheath). Scatterplots of *g*-ratio as

a function of axon caliber are shown comparing optogenetically stimulated mice vs. identically manipulated WT controls for each genotype studied.

A) A scatterplot of all axons measured shows an increase in myelin sheath thickness (reduced *g*-ratio) in *Bdnf*^{WT}*;Thy1::ChR2*$^{+/-}$ (n=5 mice; red triangles) mice compared to *Bdnf*^{WT}*;*WT (n=5 mice; black triangles).

B) A scatterplot of all axons measured show no difference in *g*-ratio between *Bdnf*^{TMKI}*;*WT (n=5 mice; black triangles) vs. *Bdnf*^{TMKI}*;Thy1::ChR2*$^{+/-}$ (n=5 mice; red triangles).

C) *g*-ratio data of *Bdnf*^{TMKI} model are shown by axon size bins of small (<0.5μm), medium (0.5-1.0 μm) and large (>1.0μm) axons.

D) A scatterplot of all axons measured shows an increase in myelin sheath thickness (reduced *g*-ratio) in TrkB WT;WT (n=6 mice; black triangles) compared to TrkB WT*;Thy1::ChR2*$^{+/-}$ (n=6 mice; red triangles).

E) A scatterplot of all axons measured show no difference in *g*-ratio between OPC-TrkB cKO;WT (n=5 mice; black triangles) compared to OPC-TrkB cKO*;Thy1::ChR2*$^{+/-}$ mice (n=5 mice; red triangles).

F) *g*-ratio data of OPC-TrkB cKO model are shown by axon size bins of small (<0.5μm), medium (0.5-1.0 μm) and large (>1.0μm) axons.

A single point indicates the *g*-ratio for a single axon. Approximately 100 axons were quantified and the mean g-ratio determined for each mouse. P-values (indicated on plots) were determined by two-way ANOVA with Tukey post-hoc analysis for multiple comparisons, comparing the mean *g*-ratio per mouse between groups.

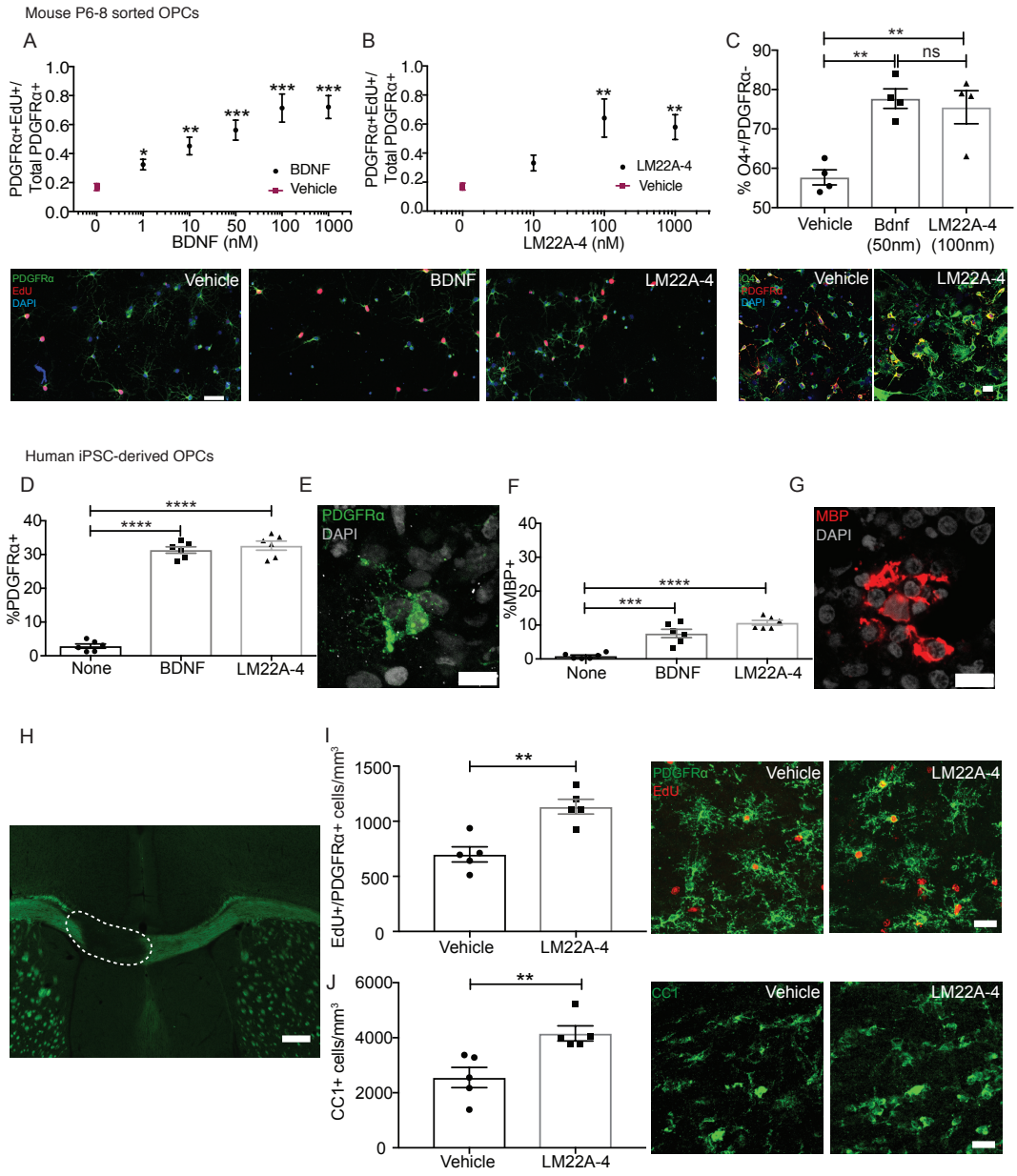

Supplemental Fig 5. A small molecule TrkB partial agonist recapitulates the effects of BDNF on OPC proliferation and oligodendrogenesis, related to Figure 6

A) Six-point dose response curve demonstrating OPC proliferation index as measured by the fraction of PDGFRα^{+}cells that co-label with EdU in P6-8 mouse OPCs at 24h after exposure to recombinant BDNF at a 0 to 1000 nM concentration range (n=6 wells per condition).

B) Four-point dose response curve demonstrating OPC proliferation index as measured by the fraction of PDGFRα^{+} cells that co-label with EdU in P6-8 mouse OPCs at 24h after exposure to LM22A-4 at a 0 to1000 nM concentration range (n=6 wells per condition).

A-B) Representative confocal images (below) of PDGFRα$^+$ (green), EdU$^+$ (red) and DAPI$^+$ (blue) vehicle control, BDNF- and LM22A-4 -treated cells. Scale bar=50μm.

C) Percent of total DAPI$^+$ cells that express O4$^+$ and do not express PDGFRα$^+$ increases at 48h after treatment of P6-8 mouse OPCs with BDNF (50nM) or LM22A-4 (100nM; n=4 wells per condition). Representative confocal images (below) of PDGFRα$^+$ (red), O4$^+$ (green) and DAPI$^+$ (blue) of vehicle control (left) and LM22A-4- treated (right) cells. Scale bar =20μm

D) Human iPS cells were treated with one of three treatment paradigms from day 25-35 in the OPC induction protocol: no BDNF, 20ng/ml BDNF as per standard protocol, or BDNF was replaced with 1000nM LM22A-4. Cells were fixed at day 100 following induction and the percent of DAPI$^+$ cells expressing the OPC marker PDGFRα was quantified.

E) Representative image of a human iPS cell-derived PDGFRα$^+$ OPC. Green = PDGFRα, white = DAPI. Scale bar =10μm.

F) Human iPS cells were treated with one of three treatment paradigms from day 25-35 in the OPC induction protocol: no BDNF, 20ng/ml BDNF as per standard protocol, or BDNF was replaced with 1000nM LM22A-4. Cells were fixed at day 100 following induction and the percent of DAPI$^+$ cells expressing the mature oligodendrocyte marker myelin basic protein (MBP) was quantified.

G) Representative image of a human iPSC-derived MBP$^+$ oligodendrocyte. Red = MBP, white = DAPI. Scale bar = 10μm.

H) Representative image of lysolecithin-induced demyelination in the corpus callosum 10 days after injection. Green = fluoromyelin stain to demonstrate myelinated architecture. White-dashed circle = lesioned area in the corpus callosum. Scale bar = 100μm.

I) Density of EdU$^+$/PDGFRα$^+$ proliferating OPCs in the corpus callosum of mice treated with 50mg/kg LM22A-4 or vehicle control for 7 consecutive days beginning 7 days after lysolecithin injection (n=5 mice/group). Representative confocal images (at right) of PDGFRα$^+$ (green) and EdU$^+$ (red) OPCs in lesioned area of vehicle control (left) and LM22A-4 -treated (right) mice. Scale bar = 20μm.

J) Density of CC1$^+$ oligodendrocyte cells in the corpus callosum of mice treated with LM22A-4 (50mg/kg) or vehicle control for 14 consecutive days beginning 7 days after lysolecithin injection (n=5 mice/group). Representative confocal images (at right) of CC1$^+$ (green) oligodendrocytes in lesioned area of vehicle control (left) and LM22A-4-treated (right) mice. Scale bar = 20μm.

Data shown as mean ± SEM. Each point = one mouse (I-J). ns = $p > 0.05$, * $p < 0.05$, ** $p < 0.01$, *** $p<0.001$, **** $p<0.0001$ as determined by one-way ANOVA (A-F) or Student's t-test (I-J).

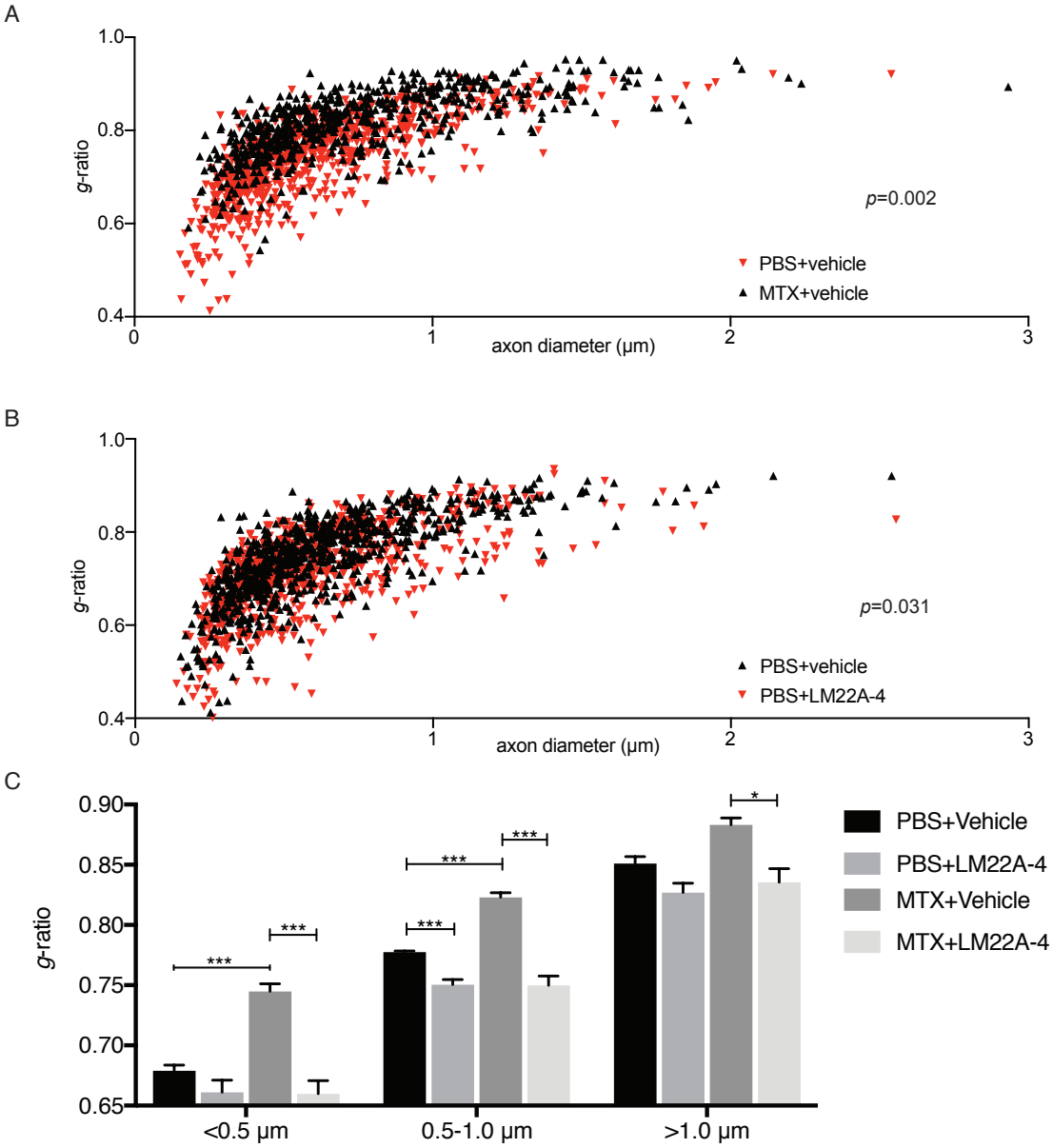

Supplemental Fig 6. TrkB partial agonist LM22A-4 normalizes myelination after methotrexate chemotherapy exposure, related to Figure 6

A) MTX-treated mice exhibit thinner myelin compared to PBS vehicle-treated controls. *g*-ratio values as a function of axon caliber are shown as a scatterplot of all axons measured in mice treated with vehicle controls for both MTX and LM2A-4 (PBS vehicle control+vehicle control; n=4 mice; red triangles) vs. MTX+vehicle control (n=4 mice; black triangles).

B) LM22A-4 increases myelin sheath thickness in control mice. *g*-ratio values as a function of axon caliber are shown as a scatterplot of all axons measured in mice treated with PBS vehicle control+vehicle control (n=4 mice; black triangles) vs PBS vehicle control +LM22A-4 (n=4 mice; red triangles).

C) *g*-ratio data shown in Figure 6 are shown by axon size bins of small (<0.5μm), medium (0.5-1.0 μm) and large (>1.0μm) axons. LM22A-4 rescues myelin deficits in mice exposed to juvenile MTX in small caliber axons (< 0.5μm; n=4 mice, p = 0.005), medium caliber axons (0.5μm – 1.0 μm; n= 4, p = 0.006) and large caliber axons (>1.0 μm; n=4 mice; p = 0.033) compared to mice exposed to MTX but treated with vehicle control. Data shown as mean ± SEM, * $p < 0.05$, ** $p < 0.01$, *** $p<0.001$, ns = $p > 0.05$. Two-way ANOVA with Tukey post-hoc multiple comparisons testing.

A single point indicates the *g*-ratio for a single axon. Approximately 100 axons were quantified per mouse and the mean *g*-ratio determined for each mouse. P-values (indicated on plots) were determined two-way ANOVA with Tukey post-hoc multiple comparisons testing comparing the mean *g*-ratio per mouse between groups.